Herbert Huppert: Gravity Currents & Solidification

A. Shravat and S. Barbot

January 12, 2009

This lecture discussed a number of topical problems in geological fluid mechanics. Two particular examples are covered in details in these notes: the dynamics of the grounding line of an ice sheet & shelf, and the fluid mechanics of carbon sequestration. Some further mathematical and physical details are relegated to the appendices.

1   Ice Sheet Grounding Line
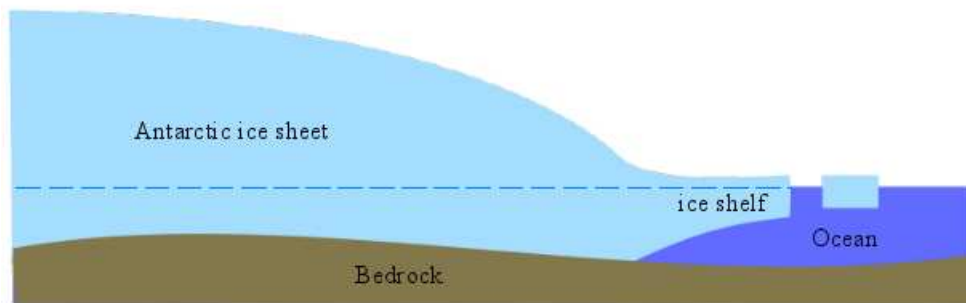
Figure 1: Ice Sheets and Ice Shelves.

In the present day, the last of Earth's large ice sheets can be found in Greenland and Antarctica. These ice sheets are continental in size and are characterized by complex dynamics that may be driven by climate forcing or the spactial and temporal variations at the ice bed or internal boundaries. Ice shelves are enormous beds of floating ice as can be seen in Figure 1 that gives a schematic view of ice sheets and shelves. Figure 2 shows photos of floating ice sheets and icebergs in the sea.

The ice sheet/ice shelf transition zone plays an important role in controlling marine ice sheet dynamics, as it determines the rate at which ice flows out of the grounded part of the ice sheet. Any change in ice thickness will of course lead to migration of the grounding line. There have been several experiments on the dynamics of the grounding line. One such experiment can be seen in Figure 3, where wax is poured over water to create a grounding line.

Figure 2: Floating ice sheets and Icebergs.
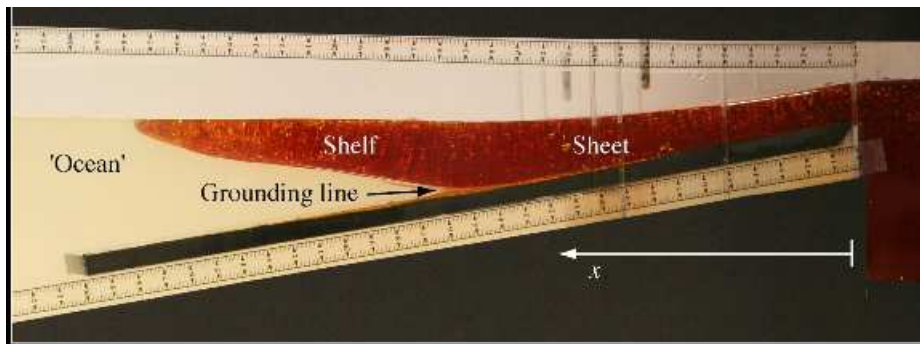
Figure 3: Laboratory experiment with wax showing the formation of the shelf.

1.1 Dynamics of Grounded Ice Sheet

The Grounded Ice Sheet can be modelled as a shear flow (see Figure 4). The dynamical balance is between the pressure gradient and the shear stress.

$$-\rho g \frac{\partial h}{\partial x} \cancel{g z} \ \mu \frac{\partial^2 u}{\partial y^2}. \tag{1}$$
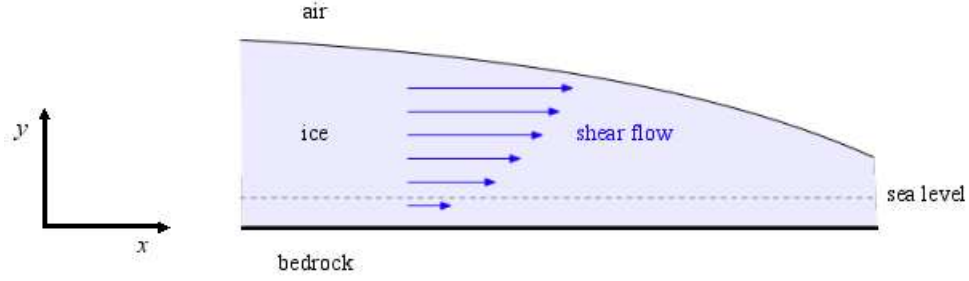
Figure 4: Schematic of the Grounded Ice Sheet.

The horizontal length scale, obtained from dimensional analysis (see section 1 in appendix A) is

$$L \sim \left(\frac{\rho g q^3}{\mu} \right)^{1/5} t^{4/5}. \tag{2}$$

where q is the precipitation rate. The horizontal length is plotted against t in Figure 5.
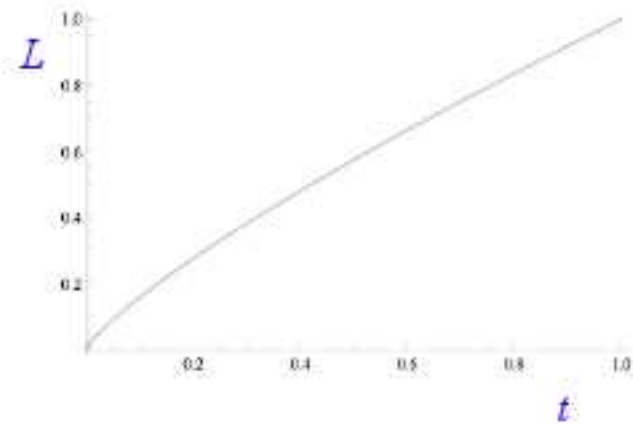
Figure 5: Plot of horizontal length scale, L against t for the grounded ice sheet.

1.2 Dynamics of Freely Floating Shelf

In the preceding section, the sheet has been modelled as fixed on a bedrock. The dynamics of a freely floating shelf shall be considered now. The leading order dynamical balance is satisfied by the pressure gradient balancing the inertia.

$$-\rho g' \frac{\partial h}{\partial x} \approx \frac{4\mu}{h} \frac{\partial}{\partial x} \left(h \frac{\partial u}{\partial x} \right), \tag{3}$$
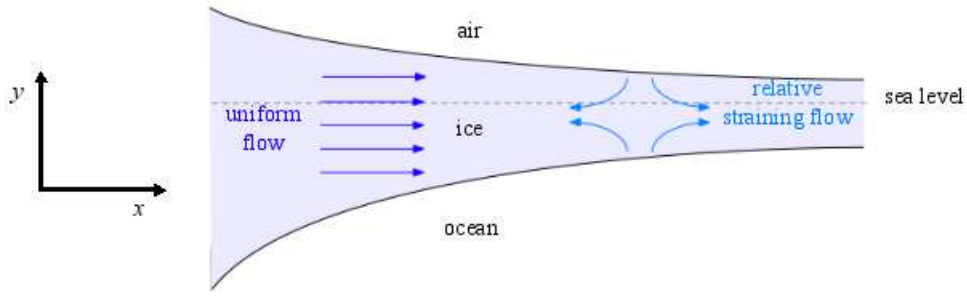
Figure 6: Schematic showing the freely floating shelf.

where $g' = \frac{\Delta\rho}{\rho}g$. The horizontal scale is given by

$$L \sim \frac{\rho g' q}{\mu} t^2. \tag{4}$$

The plot of horizontal scale, L against t is shown in Figure 7.
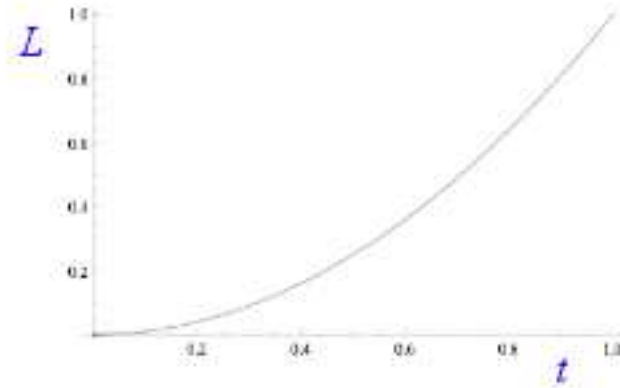
Figure 7: Graph of L against t for freely floating shelf.

1.3 Modelling Ice Sheet-Shelf Dynamics

The dynamics of both ice sheet and shelf together is considered in this section. A sketch of this with various parameters is given in Figure 8. The flux in the sheet is given by

$$q = \frac{gH^3}{3\nu}\left(-\frac{\partial h}{\partial x}\right). \tag{5}$$

Here $H = h + b$. The continuity (mass conservation) requires that

$$\frac{\partial h}{\partial t} = -\frac{\partial q}{\partial x}, \tag{6}$$

99
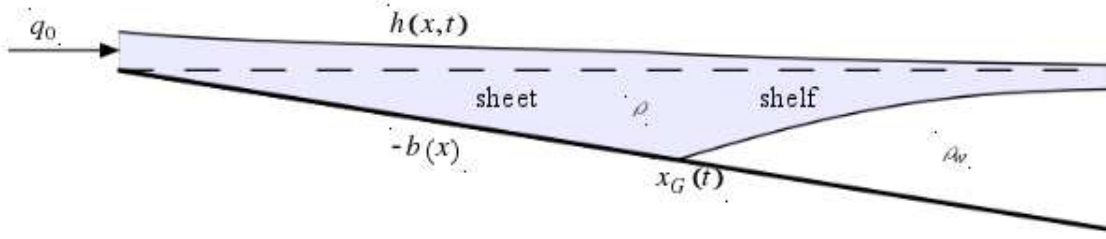
Figure 8: Schematic of the ice sheet and shelf with flux q_0 due to precipitation. The parameter $b(x)$ defines the bottom topography.

This gives rise to the nonlinear diffusion equation,

$$\frac{\partial h}{\partial t} = \frac{\partial}{\partial x}\left[\frac{g}{3\nu}(h+b)^3\frac{\partial h}{\partial x}\right]. \tag{7}$$

The prescribed volume flux (due to precipitation) at $x = 0$ is given by

$$q_0 = -\frac{g}{3\nu}h^3\frac{\partial h}{\partial x}, \tag{8}$$

The floatation condition at $x = x_G(t)$ is defined as

$$\rho H = \rho_w b, \tag{9}$$

The normal stress balance at $x = x_G(t)$ is

$$\left(\frac{\Delta\rho}{\rho}\frac{db}{dx} - \frac{\partial h}{\partial x}\right)x_G = \frac{gH^2}{8\nu}\left[4\left(\frac{\partial h}{\partial x}\right)^2 - \frac{\Delta\rho}{\rho}\right]. \tag{10}$$

Theory gives the following results:

$$x_G(t) \sim t^{1/2}, \tag{11}$$

at early times. For late times,

$$x_G(t) \to \text{constant}. \tag{12}$$

The various grounding line positions are plotted against time in Figure 9. Theory predicts the position of a steady grounding line to be

$$x_G = \frac{1}{\alpha}\frac{\rho}{\rho_w}\left(\frac{6\nu q_0}{g}\right)^{1/3}\left(\frac{g}{g'}\right)^{1/6}.$$

Figure 10 provides a comparison between the theoretical and experimental results. Figure 11 compares some of the theoretical steady profiles with actual ice sheets from Antartica.

To summarise, ice sheets and shelves flow as viscous gravity currents. In grounded ice sheets, shear stresses balance the hydrostatic pressure gradient. The result is a decelerating
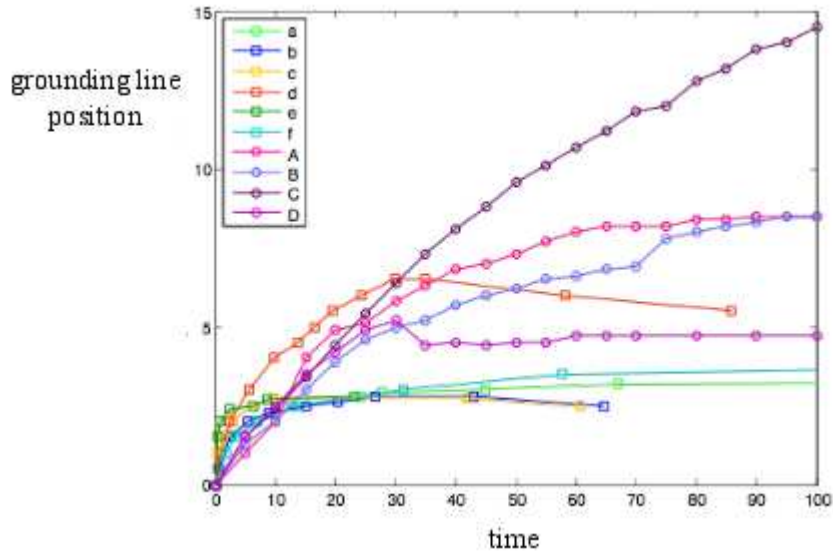
Figure 9: Plot showing the grounding line position as a function of time in the case of ice sheet-shelf dynamics.
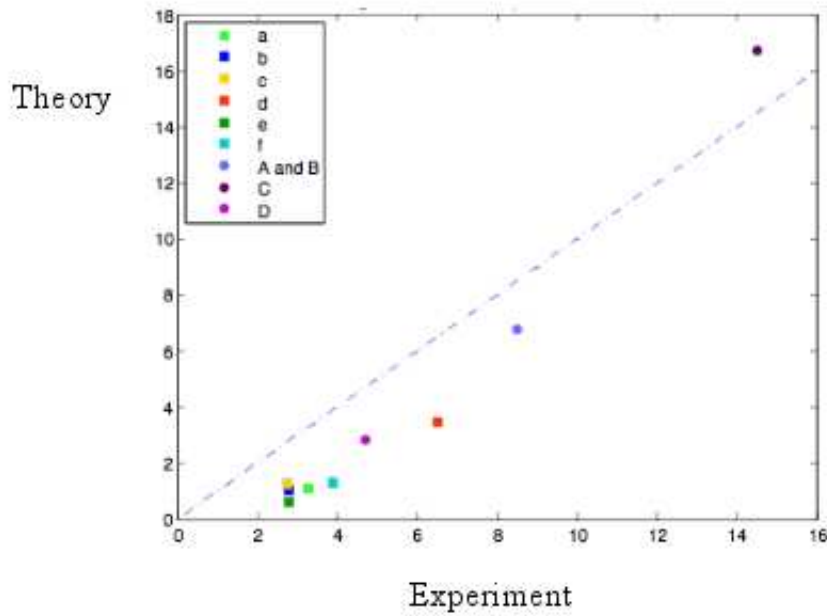
Figure 10: A comparison between theoretical prediction and experimental results for the position of the grounding line.

flow. The floating ice shelf, on the other hand, has extensional stress balancing the hydrostatic pressure gradient, causing the flow to accelerate. This gives rise to a hypothesis that
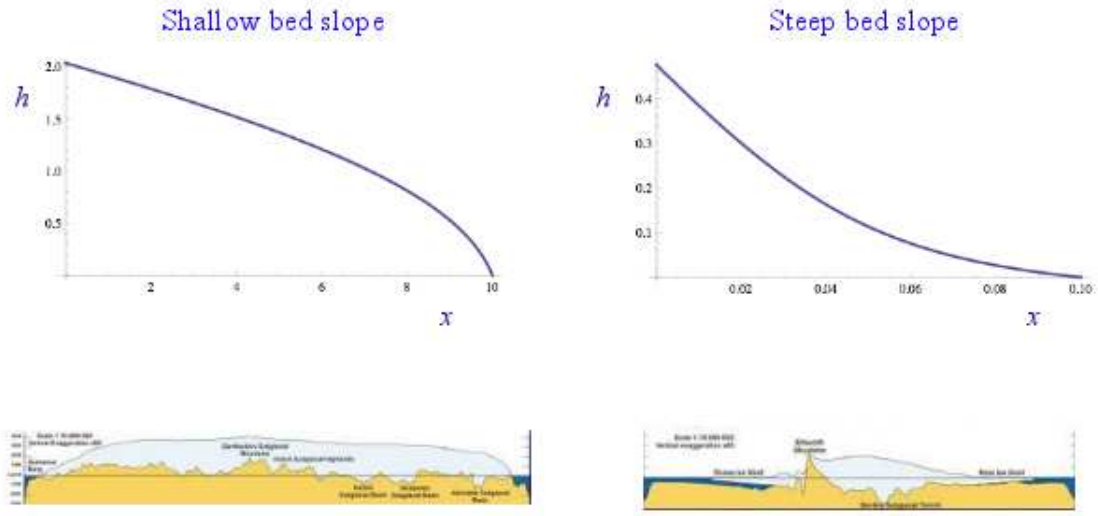
Figure 11: Steady Ice sheets with Grounding Lines.

the dynamic control of grounding line is effected by balance of normal stress. Hence, leading to a closed mathematical model. This hypothesis is being tested using laboratory experiments. One application of this mathematical model is to determine the dynamical stability of ice sheets. As mentioned earlier, grounding line is very sensitive to any change in the climate. To this end, more work is being carried out to understand the basic mechanisms determining its stability and position.

To summarize, ice sheets and shelves can be modelled as viscous gravity currents. In grounded ice sheets, shear stresses balance the hydrostatic pressure gradient. The result is a decelerating flow. The floating ice shelf, on the other hand, has extensional stress balancing the hydrostatic pressure gradient, causing the flow to accelerate. This gives rise to a hypothesis that the dynamic control of grounding line is effected by balance of normal stress. Hence, leading to a closed mathematical model. This hypothesis is being tested using laboratory experiments. One application of this mathematical model is to determine the dynamical stability of ice sheets. As mentioned earlier, grounding line is very sensitive to any change in the climate. To this end, work is being carried out to understand the basic mechanisms determining its stability and position.

2 Fluid Mechanics of Carbon Dioxide Sequestration

2.1 Introduction and Motivation

The Keeling curve (Fig. 12) is a graph showing the variation in concentration of atmospheric carbon dioxide since 1958. It is based on continuous measurements taken at the Mauna

Loa Observatory in Hawaii under the supervision of Charles D. Keeling from the Scripps Institution of Oceanography. His measurements show evidence of CO_2 undergoing a regular seasonal cycle, reflecting the seasonal growth and decay of land plants in the northern hemisphere, as well as a regular long-term rise driven by the burning of fossil fuels. Before the industrial era, atmospheric CO_2 concentration was between 275 and 280 ppmv for several thousand years. Carbon dioxide has risen continuously since then, and the average value when Dr. Keeling started his measurements in 1958 was near 315 ppmv. By the year 2000 it has risen to about 367 ppmv. Keeling's measurements showed the first significant evidence of rapidly increasing carbon dioxide levels in the atmosphere.
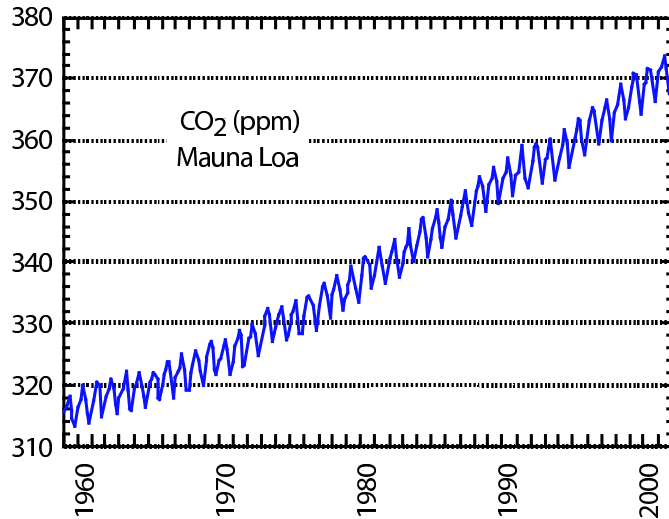
Figure 12: Keeling Curve. Atmospheric carbon dioxide concentration (ppm) above Mauna Loa observatory in Hawai.

Fig. 13 compares the world and the United States population and energy usage in 1906 and 2006. At the start of the industrial era, the world population was about one billion souls. It took 120 years to double this number. Today, at the rate about 200,000 new people per day, it takes 13 years for the world population to grow by a billion. Todays large human population and rate of growth is not without effect on the environment. Between 1906 and 2006, the U.S. as well as the world population grew nearly four fold. The world energy usage increased almost 13-fold. In the U.S. alone, energy usage in 2006 is 9 times its value in 1906.

Fig. 14 shows the source contributions of world energy consumption. Fossil fuels (coal, oil and natural gas) still account for over 85% of the primary energy consumed in the world. Fossil fuels or mineral fuels are fossil source fuels, that is, hydrocarbons found within the top layer of the Earth's crust. The burning of fossil fuels produces around 21.3 billion tons of carbon dioxide per year, but it is estimated that natural processes can only absorb about half of that amount, so there is a net increase of 10.65 billion tons of atmospheric carbon dioxide per year (one ton of atmospheric carbon is equivalent to 44/12 or 3.7 tons of carbon dioxide). Carbon dioxide is one of the greenhouse gases that enhances radiative forcing and contributes to global warming, causing the average surface temperature of the Earth to rise

14

12

10

8

6

4

2

1906 2006

world pop.
(x10^9)

U.S. pop.
(x10^8)

world energy
usage (x10^{12} kWh)

U.S. energy
usage (x10^{12} kWh)
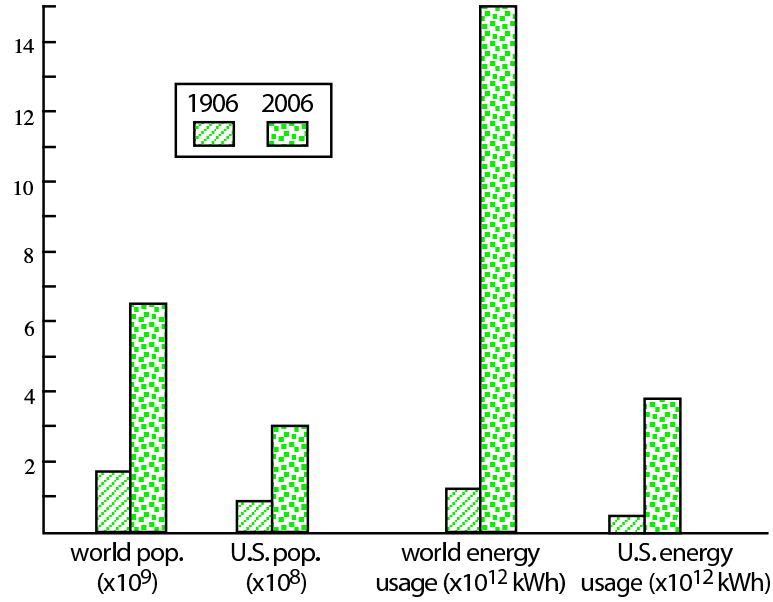
Figure 13: A hundred years evolution of the United States and the world's population and energy usage. Between 1906 and 2006, the U.S. as well as the world population grew nearly four fold. The world energy usage increased almost 13-fold. In the U.S. alone, energy usage in 2006 is 9 times its value in 1906.

in response.

In the last 400,000 years temperature was highly correlated with CO_2 concentration in the atmosphere. Inferred mean temperature anomalies (difference with present time) exhibit a roughly 100,000 year cycle with amplitude varying from -6 °C to +2 °C. Effect of strong increase of CO_2 in the atmosphere is associated with climate change. Long records of carbon dioxide concentration in the atmosphere indicate that CO_2 content never exceeded 300 ppm in the last 400,000 years. The amplitude of the sudden increase of CO_2 concentration in the last hundred years, associated with burning of fossil fuel, is unprecedented in recent geological history. The effects, mechanisms and time scales of climate change are subject to active research. Limiting the effects of human activities on the environment involves a migration to renewable energies and the reject of fossil fuel as a primary source of energy. One way to reverse the Keeling curve, however, to return to geologically normal atmospheric carbon dioxide concentration, is to the re-injection of CO_2 in underground reservoirs. The so called carbon dioxide sequestration provides means to remove CO_2 from the atmosphere and restore the status quo of pre-industrial era. The problem of carbon dioxide sequestration calls for further investigation of the behavior of gravity (buoyancy) driven flows in porous media.

2.2 Source in Porous Medium

Flow in porous media occurs in many natural and industrial situations. Included in these are the seepage of rainwater through permeable ground into an aquifer, the forced flow of
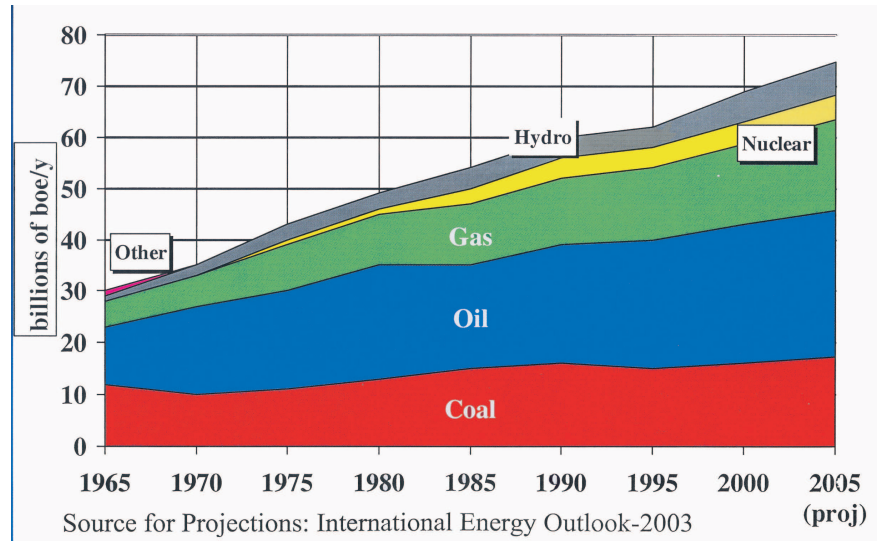
Figure 14: Distribution of energy source over the last five decades. Fossil fuels still account for over 85% of the primary energy consumed in the world.
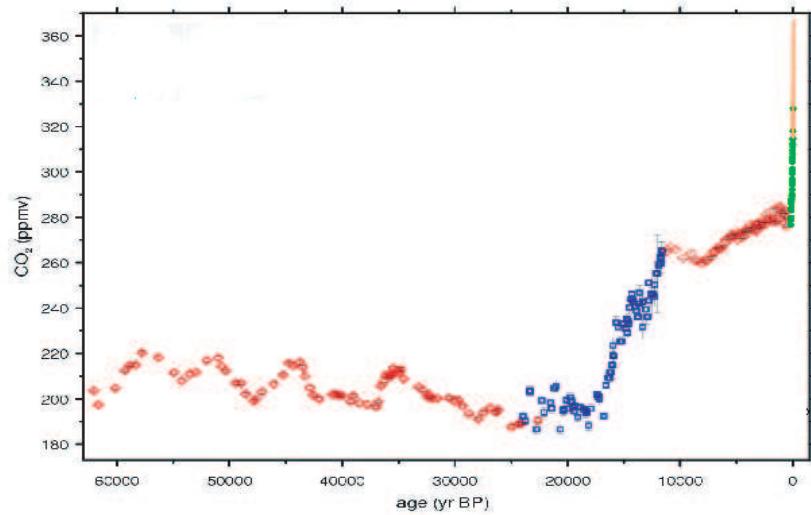
Figure 15: Carbon dioxide levels over the last 60,000 years in volume ppm. Longer records show that CO_2 concentration did not exceed 300 ppm in the last 400,000 years. Observed increase in CO_2 content in the last hundred years is unpreeceded in recent geological history.

Figure 16: Schematic of gravity fluid in a porous medium.

oil from sandstone reservoirs (Lake 1989; Gerritsen & Durlofsky 2005), and the dispersion of polluted liquids through gravel pits. In some situations the fixed, solid matrix through which the flow passes reacts with the interstitial fluid and the structure and porosity of the matrix change with position and time (Hallworth, Huppert & Woods 2005). Examples of such reactions include the gradual formation of dolomite (Phillips 1991) and the convective flow due to solidification through a mushy layer, which is a region of reactive solid matrix bathed in interstitial fluid (Worster 2000; Aussillous et al. 2006).

A gravity current occurs whenever fluid intrudes primarily horizontally into fluid of different density. The fundamentals of flows beneath a relatively less dense homogeneous fluid layer at either low (Huppert 1982a, b, 2000) or high Reynolds number (Benjamin 1968; Hoult 1972) are well known. In recent years additional phenomena due to the effects of rotation (Ungarish & Huppert 1998), and flows over porous media (Acton, Huppert & Worster 2001; Thomas, Marino & Linden 2004), into stratified ambients (Ungarish & Huppert 2002; Maxworthy et al. 2002) and over variable topography have been investigated.

The spreading of a liquid phase in a porous medium hosting pore fluid of different density, as sketched in Fig. 16, is a kind of gravity current. Consider the gravity current due to horizontal pressure gradient of (unknown) free surface slope (see also Appendix A). The dynamics of the fluid is simplified to the viscous approximation (Darcy's flow)

$$0 = -\nabla p - \rho \mathbf{g} - \mu \mathbf{u}/k \tag{13}$$

where k is the porous medium permeability, μ is the dynamic viscosity of input fluid and $\mathbf{u}$ is the input fluid velocity. In the horizontal direction, this becomes

$$\frac{\partial p}{\partial r} = \rho \, g' \frac{\partial h}{\partial r} \tag{14}$$

where

$$g' = g \frac{\Delta \rho}{\rho} \tag{15}$$

is the reduced gravity. The equation of local continuity gives

$$\phi \frac{\partial h}{\partial t} + \frac{1}{r} \frac{\partial}{\partial r} (r \, u \, h) = 0 \tag{16}$$

106

where ϕ is the porosity of the host rock. Equating the last two equalities gives

$$\frac{\partial h}{\partial t} - \frac{\gamma}{r}\frac{\partial}{\partial r}\left(r\,h\,\frac{\partial h}{\partial r}\right) = 0 \tag{17}$$

and

$$\gamma = \frac{\rho\,k\,g'}{\phi\,\mu} \tag{18}$$

has the dimensions of a velocity. The equation of global continuity gives

$$Q\,t = 2\pi \int_0^{r_N(t)} r\,h\,dr \tag{19}$$

The similarity variable

$$\eta = (\gamma\,Q/\phi)^{-1/4}\,r\,t^{-1/2} \tag{20}$$

leads to an expression for the position of the nose

$$r_N(t) = \eta_N(\gamma\,Q/\phi)^{1/4}\,t^{1/2} \tag{21}$$

Defining $y = \eta(r,t)/\eta(r_N,t)$ with $0 < y < 1$ and

$$h(r,t) = \eta_N^2\,(Q/\phi\gamma)^{1/2}\,f(y) \tag{22}$$

one obtains the ordinary differential equation

$$(y\,f\,f')' + \frac{1}{2}y^2\,f' = 0 \tag{23}$$

with $f(1) = 0$ and

$$\eta_N = \left[2\pi \int_0^1 y\,f(y)\,dy\right]^{-1/4} \tag{24}$$

For a linear case, with $Q = 0$, approximation solution of the differential equation gives

$$f(y) \sim \frac{1}{2}(1 - y) \tag{25}$$

and

$$\eta_N \sim (6/\pi)^{1/4} \tag{26}$$

Data from laboratory experiments are well explained by such scaling. Further experiments on gravity currents in porous media may help us predict the fate of liquid phase carbon dioxide injected in porous reservoirs (Fig. 17).
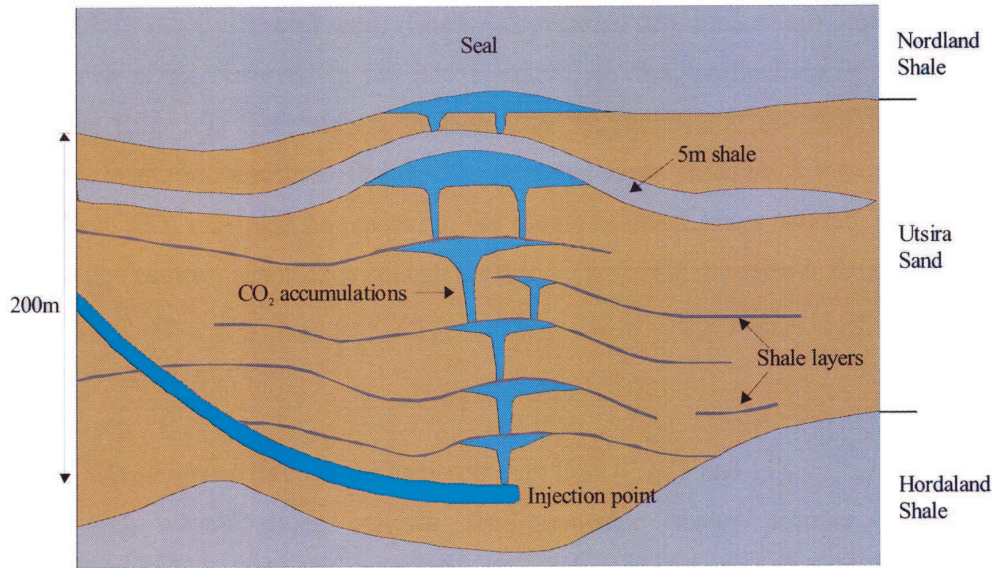
Figure 17: Schematic of carbon dioxide (liquid phase) sequestration and propagation in a porous reservoir
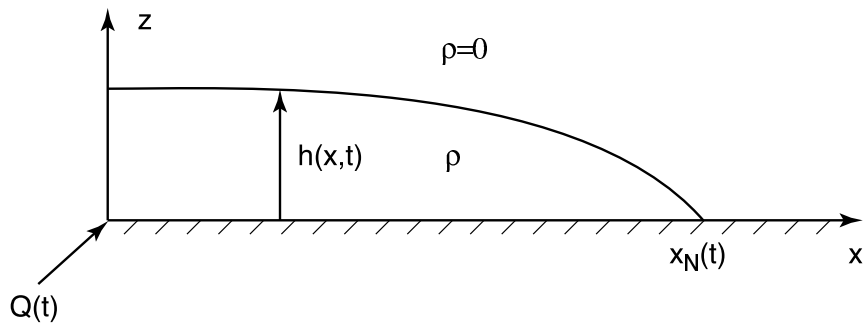
Figure 18: Gravity current model. The flow is driven by pressure gradient due to unknown free surface slope and resisted by viscosity.

Appendices

A   Gravity Currents

Gravity currents are generated by the release of some volume of one homogeneous fluid into another of slightly different density. If a viscous fluid is released vertically on a horizontal surface it rapidly takes up a circular plan form as it spreads. This form is observed to be stable to any small disturbances which are initiated on the front due, for example, to irregularities in the horizontal surface or to chance perturbations (Huppert 1980, Huppert 1982a). In this note, we describe how gravity currents spread, and quantify their radius or extent as a function of time.

We consider that the flow is driven by pressure gradient due to unknown free-surface slope $h(x,t)$ and resisted by viscous effects. We first examine a two-dimensional flow propagating in the x-direction only, with a vertical dependence. Model geometry is illustrated in Fig. 18. Assuming the velocity field $\mathbf{u} = u_x(x,z)\,\mathbf{e}_x$, the Navier-Stokes equation can be written

$$\mu\,\frac{\partial^2}{\partial z^2}u = -\frac{\partial}{\partial x}p = \rho\,g\,\frac{\partial}{\partial x}h \tag{27}$$

where we have ignored inertial effects (Reynolds number $\mathrm{Re} \ll 1$), μ is the dynamic viscosity and p is pressure. Also assumed is a thin layer where $u_{zz} \gg u_{xx}$.

A.1   Dimensional analysis

As shown in Fig. 18, the flow is sustained by the mass flux $\rho\,Q(t)$. Experimental data indicates the time dependence

$$H\,L \;\sim\; \int_0^t Q(t')dt' \;\sim\; q\,t^\alpha \tag{28}$$

where H, L are typical height and typical length and α is a constant. For $\alpha = 0$, the volume is constant. The case $\alpha = 1$ corresponds to constant flux. Using dimension analysis, one can write orders of magnitude of the total buoyancy force F_g

$$\begin{aligned}
F_g &= \iiint_V \frac{\partial p}{\partial x}\,dx\,dy\,dz \\
&= -\rho\,g \iiint_V \frac{\partial h}{\partial x}\,dx\,dy\,dz \\
&\sim \rho\,g\,H^2 W \\
&\sim (\rho\,g\,q^2\,W/L^2)\,t^{2\alpha}
\end{aligned} \tag{29}$$

and the total viscous force F_ν

$$\begin{aligned}
F_\nu &= \mu \iiint_V \frac{\partial^2 u}{\partial z^2}\,dx\,dy\,dz \\
&\sim \mu\,ULW/H \\
&\sim \mu\,q^{-1}L^3 W t^{-\alpha-1}
\end{aligned} \tag{30}$$
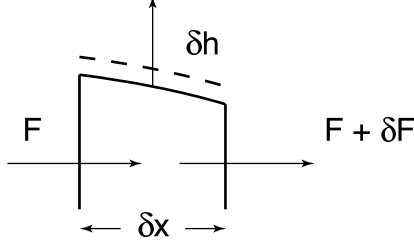
Figure 19: The continuity equation. The change in velocity flux $\mathcal{F}$ is balanced by the change in unknown elevation h.

The buoyancy and viscous forces balance ($F_\nu \sim F_g$) leading to an estimate of the total extension of the gravity flow

$$L = (g\,q^3/\nu)^{1/5} t^{(3\alpha+1)/5} \tag{31}$$

A.2 Lubrication theory analysis

We use the approximations of lubrication theory, where we neglect both surface tension and contact line effects (Hocking 1981). Both can be neglected if the Bond number

$$B = \rho\,g\,l^2/T \gg 1 \tag{32}$$

where ρ is the density of the fluid, l is a representative length scale of the current, and T is the surface tension. Using the x-momentum equation, and the thin layer approximation $u_{xx} = 0$, one obtains

$$\frac{\partial^2}{\partial z^2}u = \frac{\rho\,g}{\mu}\frac{\partial}{\partial x}h \tag{33}$$

We consider the boundary conditions

$$\begin{aligned}
u &= 0, \quad \text{at } z = 0 \\
u_z &= 0, \quad \text{at } z = h
\end{aligned} \tag{34}$$

The solution velocity is

$$u(x,z,t) = -\frac{g}{2\,\nu}\frac{\partial h}{\partial x}z(2h-z) \tag{35}$$

where $\nu = \mu/\rho$ is the kinematic viscosity. The velocity flux is

$$\mathcal{F} = \int_0^h u\,dz = -\frac{1}{3}\frac{g}{\nu}h^3\frac{\partial h}{\partial x} \tag{36}$$

The velocity flux has the dimensions of $\mathcal{F} \sim L^2\,T^{-1}$. Another constraint of the problem is the conservation of mass. The local continuity requires that the difference in velocity flux between to neighboring columns is balanced by the change of height

$$\partial h \partial x + \partial \mathcal{F} \partial t = 0 \tag{37}$$

110

or

$$\frac{\partial \mathcal{F}}{\partial x} + \frac{\partial h}{\partial t} = 0 \tag{38}$$

Using equation (36), one obtains

$$\frac{\partial h}{\partial t} - \beta \frac{\partial}{\partial x}\left(h^3 \frac{\partial h}{\partial x}\right) = 0 \tag{39}$$

where $\beta = g/3\nu$. Equation (39) corresponds to the nonlinear diffusion equation. The global continuity equation can be written

$$\int_0^{x_N(t)} h(x,t)\, dx = q\, t^\alpha \tag{40}$$

where $q\, t^\alpha$ corresponds to the cumulative (with time) influx of material volume. The method used by H^2 to determine a similarity solution is to write down the governing equation in terms of dimension. Equation (39) can leads to

$$\frac{h}{t} \sim \frac{\beta\, h^4}{x^2} \quad \text{or} \quad h^3 \sim \frac{x^2}{\beta t} \tag{41}$$

now assuming no influx of mass ($\alpha = 0$), and a conserved area A, one has $h\, x_N \sim A$. So one gets

$$\frac{x^5}{\beta\, A^3\, t} \sim 1 \tag{42}$$

which suggests the following dimensionless quantity

$$\eta = (\beta\, A^3)^{1/5}\, x\, t^{-1/5} \tag{43}$$

to be suitable for similarity variable. One obtains the estimate

$$x_N \sim (\beta\, A^3)^{1/5}\, t^{1/5} \tag{44}$$

Introducing η_N, the value of η at the nose ($x = x_N$) of the current, and using

$$h \sim \frac{A}{x_N} \sim \left(\frac{A^2}{\beta}\right)^{1/5} t^{-1/5} \tag{45}$$

we use the change of variable

$$h(x,t) = \eta_N^{2/3}(A^2/\beta)^{1/5} t^{-1/5}\, \phi(\eta/\eta_N) \tag{46}$$

and we further define $y \equiv \eta/\eta_N$ with $0 < y < 1$. The partial derivatives become

$$\begin{aligned}
\partial_t &= d_t - \frac{1}{5}\frac{y}{t} d_y \\
\partial_x &= \frac{y}{x} d_y
\end{aligned} \tag{47}$$

111

For example, one has

$$h_t = \eta_N^{2/3}(A^2/\beta)^{1/5}\left\{\frac{1}{5}t^{-4/5}\phi + yt^{-4/5}\phi'\right\} \tag{48}$$

The partial differential equation governing the height of the gravity current becomes the ordinary differential equation

$$(\phi^3\,\phi')' + \frac{1}{5}\phi' + \frac{1}{5}\phi = 0 \tag{49}$$

with the boundary conditions $\phi = 0$ and regular at $y = 1$. Integrating twice, we find

$$\phi(y) = \left(\frac{3}{10}\right)^{1/3}(1 - y^2)^{1/3} \tag{50}$$

and $\eta_N = 1.411$. We find that the problem is not solvable analytically for $\alpha \neq 0$. In general however, one has

$$x_N = \eta_N\left(\beta\,q^3\right)^{1/5}t^{(3\alpha+1)/5} \tag{51}$$

Above theory agrees with experiments.

B   Solidification

Solidification is the growth of a solid from a liquid phase. It is an important processing route for metals and alloys and has a number of important geological problems associated with it. In most geological problems, it is assumed that the magma has a well-defined melt temperature at which the phase change from liquid to solid occurs. The problem of solidification can be defined by Stefan's condition. The Stefan condition for heat flux $\mathbf{q}$ and velocity of solidification V_n is given by

$$\rho_s L V_n = [\mathbf{n},\ \mathbf{q}]. \tag{52}$$

where L is the latent heat per unit mass, ρ_s is the density of the solid and $\mathbf{n}$ is the normal to the surface. Operator $[\mathbf{a},\ \mathbf{b}]$ implies the difference between $\mathbf{a} \cdot \mathbf{b}$ on either side of the solid-liquid interface, where a discontinuity in temperature gradient occurs. The location of the phase change boundary or the interface between the solid and liquid is determined as part of the solution. A complication, however, is the changing of this boundary as solidification proceeds. Another difficulty is to keep track of the latent heat of fusion, which is located at the solid-liquid interface as solidification takes place.

B.1   Planar 1-component solidification

Sometimes the solidification occurs in organised planar way. An example of such solidification is that of a horizontal layer of magma that solidifies from its upper surface downwards as a result of being cooled from above. In this case, the overall flow thickness is unimportant in describing the solidification process as long as a molten region is present. The planar 1-component solidification is given by the equation (53), where T is the temperature.
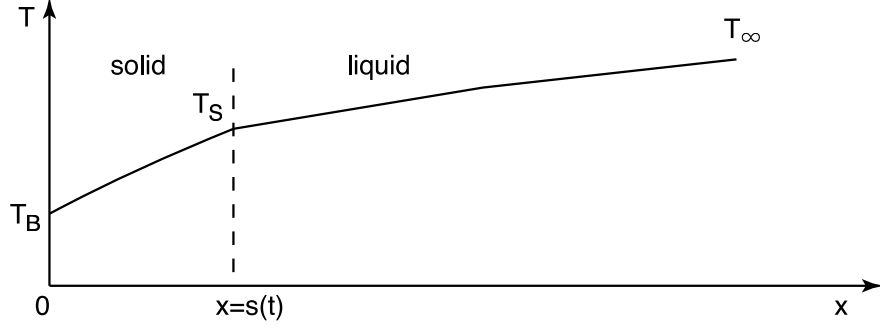
Figure 20: Schematic showing the interface between Solid and Liquid with the boundaries at $x = 0$ and $x = s(t)$. For simplicity material properties are assumed equal.

$$T_t = \kappa T_{xx} \tag{53}$$

where κ is thermal diffusivity. The boundary conditions are:

$$T = T_B \text{ at } x = 0,$$

$$T = T_S \text{ at } x = s(t),$$

$$T \to \infty \text{ as } x \to \infty.$$

The Stefan's condition, (52) in this case is given by

$$\rho_s L s' = k(T_x|_{s_-} - T_x|_{s_+}). \tag{54}$$

where k is the thermal conductivity and s' is the first derivative of s with respect to t. This has similarity solution of the form

$$s(t) = 2\lambda(\kappa t)^{1/2}. \tag{55}$$

This can be represented using $\text{erf}(x)$ and λ, which is an eigenvalue of this system defined as a function of S and R. The form of the solution is given by the following expression, where λ_1 is defined as $s_m/2\sqrt{\kappa t}$. s_m gives the solidification interface.

$$\lambda = f[S, \ R], \tag{56}$$

where

$$S = \frac{L}{c(T_S - T_B)} \tag{57}$$

is the Stefan number relating latent heat to heat capacity and

$$R = \frac{T_\infty - T_S}{T_S - T_B} \tag{58}$$

is the nondimensional thermal forcing. The constant λ_1 is determined by requiring that the latent heat liberated at the solidification boundary be conducted vertically upward, away from the interface.

113

B.2 Binary alloys

Binary alloys are formed when 2 or more components melt. Sinking of salty water in polar seas or the mixing or iron and impurities in liquid outer core of the Earth are both examples of binary alloys. Figure 21 shows the Phase Diagram for Binary alloys. This representation is often correct in equilibrium but can be very different in many cases. It is worth noting that the freezing temperature (liquidus) is function of composition $T_L(C)$. The solid that freezes has a very different composition (given by solidus) than the liquid. Typically, aqueous solutions have vertical solidus.
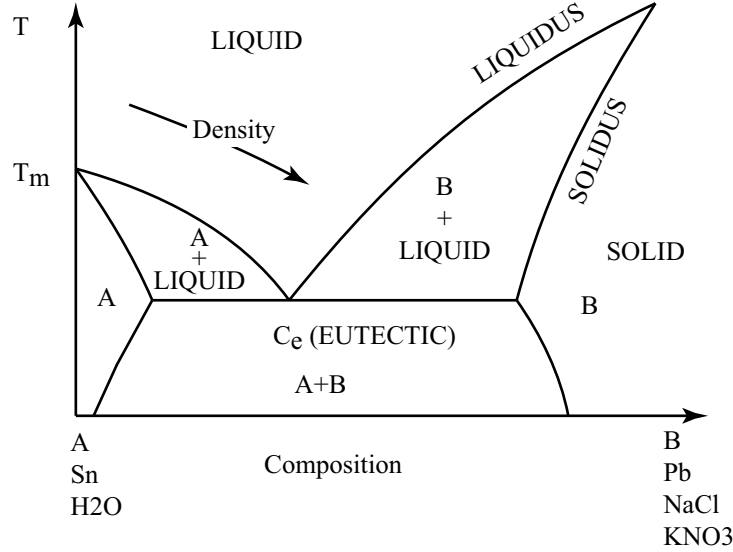
Figure 21: An equilibrium Phase Diagram for Binary Alloys.

B.2.1 Stefan Problem for an alloy

This problem is similar to the Planar 1-component solidification. The equilibrium liquidus can be written as

$$T_i = T_L(C_i). \tag{59}$$

The Stefan condition is

$$\rho_s L s' = -[kT_x]_s^l. \tag{60}$$

The solute conservation is given by

$$(C_i - C_s)s' = -DC_x|_{s_+}. \tag{61}$$

The governing differential can be written in terms of T_t and C_t.

$$T_t = \kappa T_{xx}, \tag{62}$$

$$C_t = DC_{xx}. \tag{63}$$

where D is the diffusion coefficient of C, typically $D \ll \kappa$. Similarity solution can be found of the form

$$s(t) = 2\mu(Dt)^n.$$

The solidification rate is controlled by the concentration diffusion. This is morphologically unstable leading to 'Mushy Layers', which are small scale reactive matrix bathed in interstitial liquid. An example of mushy layer is sea ice. Seeking averaged description of local mean temperature $(T(\mathbf{x},t))$, mean composition of interstitial liquid $(C(\mathbf{x},t))$ and solid fraction $(\phi(\mathbf{x},t))$ leads to the equations for the Mushy layer.

$$\bar{\rho}c(T_t + \mathbf{u}.\nabla T) = \nabla.(\bar{k}\nabla T) + \rho_s L\phi_t, \tag{64}$$

$$(1 - \phi)(C_t + \mathbf{u}.\nabla C) = \nabla.(\bar{D}\nabla C) + (C - C_s)\phi_t. \tag{65}$$

At equilibrium,

$$T = T_L(C).$$

It is safe to say that multicomponent melts solidify into mushy layers, which are often accompanied by strong compositional convection. In many circumstances, it is possible quantitatively to predict structure and rate of growth of mushy layers. An example of solidification is the almost pure iron inner core that has been slowly solidifying for about 1.8×10^9 years (just under half the age of the Earth). During all this time strong compositional convection has maintained the geodynamo protecting us from cosmic radiation.

References

[1] J. M. Acton, H. E. Huppert & M. G. Worster, *Two-dimensional viscous gravity currents flowing over a deep porous medium*, J. Fluid Mech., 440 (2001), pp. 359-380.

[2] P. Aussillous, A. J. Sederman, A. Gladden, H. E. Huppert & M. G. Worster, *Magnetic resonance imaging of structure and convection in solidifying mushy layers*, J. Fluid Mech., 552 (2006), pp. 99-125

[3] T. B. Benjamin, *Gravity currents and related phenomena*, J. Fluid Mech., 31 (1968), pp. 209–248.

[4] M. G. Gerritsen & L. J. Durlofsky, *Modelling fluid flow in oil reservoirs*, Ann. Rev. Fluid Mech., 37 (2005), pp. 211–238.

[5] M. A. Hallworth, H. E. Huppert and A. W Woods, *Dissolution-driven convection in a reactive porous medium*, J. Fluid Mech., 535 (2005), pp. 255-285.

[6] L. M. Hocking, *Sliding and spreading of thin two-dimensional drops*, Q. J. Mech. Appl. Math., 1 (1981), pp. 37–55.

[7] D. P. Hoult, *Oil spreading on the ocean*, Ann. Rev. Fluid Mech., 4 (1972), pp. 341–368.

[8] H. E. Huppert, *Geological Fluid Mechanics.* In *Perspectives in Fluid Dynamics: A collective introduction to current research.* Eds. G.K. Batchelor, H.K. Moffatt & M.G. Worster. pp. 447-506 (2000; C. U. P.)

[9] H. E. HUPPERT, *The propagation of two-dimensional and axisymmetric viscous gravity currents over a rigid horizontal surface*, J. Fluid Mech., 121 (1982a), pp. 43-58

[10] H. E. HUPPERT, *Flow and instability of a viscous current down a slope*, Nature, 300 (1982b), pp. 427–429.

[11] H. E. HUPPERT AND J. E. SIMPSON, *The slumping of gravity currents*, J. Fluid Mech., 99 (1980), pp. 785–799.

[12] L. W. LAKE, *Enhanced oil recovery* (1989; Prentice Hall)

[13] T. MAXWORTHY, J. LEILICH, J. E. SIMPSON & E. H. MEIBURG, *The propagation of a gravity current in a linearly stratified fluid*, J. Fluid Mech., 453 (2002), pp. 371-394.

[14] L. P. THOMAS, B. M. MARINO & P. F. LINDEN, *Lock-release inertial gravity currents over a thick porous layer*, J. Fluid Mech., 503 (2004), pp. 291-319.

[15] M. UNGARISH & H. E. HUPPERT, *The effects of rotation on axisymmetric, particle-driven gravity currents*, J. Fluid Mech., 362 (1998), pp. 17-51.

[16] M. UNGARISH & H. E. HUPPERT, *On gravity currents propagating at the base of a stratified ambient*, J. Fluid Mech., 458 (2002), pp. 282-301.

[17] M. G. WORSTER, *Solidification in fluids.* In *Perspectives in Fluid Dynamics: A collective introduction to current research.* Eds. G.K. Batchelor, H.K. Moffatt & M.G. Worster. pp. 393-446 (2000; C. U. P.)